Intelligent Systems with Applications 16 (2022) 200123

Contents lists available at ScienceDirect

Intelligent Systems with Applications

journal homepage: www.journals.elsevier.com/intelligent-systems-with-applications

Novel uterine contraction signals decomposition for enhanced preterm and birth imminency prediction

Ejay Nsugbe

Nsugbe Research Labs, Swindon SN1 3LG, United Kingdom

ARTICLE INFO

Keywords:
Preterm prediction
Machine learning
Signal processing
Decision support
Intelligent systems
Cybernetics

ABSTRACT

Preterm births are one of the key causes of death in children under the age of five: they have financial implications associated with care and cause great psychological distress for the families involved. In this work, we applied a novel signal decomposition approach termed Linear Series Decomposition Learner (LSDL) from electrohysterogram (EHG) and tocodynamometer (Toco) signals to the prediction of a preterm delivery, alongside an associated delivery imminency timeline, using the logistic regression and support vector machine classifiers. The results from the classification exercise showed an equivalent performance for the EHG and Toco signals for the preterm prediction, while in the case of the imminency prediction, the Toco signals provided better results in predicting the delivery imminency period. These results have made apparent that a LSDL decomposed Toco/mechanical signal carries useful information which can be used to predict delivery imminency and supersedes that of an electrophysiological/EHG signal.

1. Introduction

A preterm birth delivery can be described as one where birth occurs before the 37th week of gestation – it has been declared by the World Health Organisation (WHO) as one of the primary causes of death in children under the age of 5 (Offiah et al., 2012; PMNCH 2012 Progress Report, 2012). Lifelong effects of a preterm birth to both child and family include physical and neurological ailments, in addition to the accompanying socioeconomic factors. The associated cost of providing care for preterm patients have also been seen to be substantial: in the UK and US costs of preterm care have been seen to be up to £95k and $100k respectively depending on the preterm severity, and false positive preterm predictions also contribute towards the overarching costs associated with preterm conditions (*Gestation-Specific Infant Mortality in England and Wales: 2011*, 2013; Greenough, 2012). Financial based theoretical modelling studies have been conducted in the literature where it has been seen that for a region which potentially delivers 180, 000 preterm babies a year, a cost saving benefit of up to €14m can be achieved with the integration of an effective preterm prediction framework within a clinical setting (Frey & Klebanoff, 2016; van Baaren et al., 2013).

As per the literature, the cause of preterm can be viewed as a problem which spans a multivariate input space, which comprises of physical factors such as early contractions, cervical weakening and membrane rupture, while lifestyle factors such as high use of drugs and alcohol have been seen to be contributors (Marshall, 1962; Nikolova et al., 2015; Paternoster et al., 2009; Rabotti & Mischi, 2015). Current means of predicting preterm delivery are primarily centred on subjective assessment of factors such as cervical length, biochemical markers such as amniotic fluids and a contraction frequency assessment (Marshall, 1962; Nikolova et al., 2015; Paternoster et al., 2009; Rabotti & Mischi, 2015).

The uterine muscle, also known as the myometrium, comprises a multitude of cells and plays the role of foetus nourishment and ejection. Like the majority of other anatomical tissue, its contractions are accompanied by a propagation of a bioelectrical signals which are termed as action potentials (Figueroa et al., 1987; Garfield et al., 1977, 1988; Rabotti & Mischi, 2015). Despite the complex nature of the uterine muscle, the general consensus is that the associated action potential signals from uterine contraction encode key information which can be used to predict a preterm birth and an associated labour imminency period (Figueroa et al., 1987; Garfield et al., 1977, 1988; Rabotti & Mischi, 2015). Due to this, there has been a high emphasis around the acquisition and analysis of biosignals associated with uterine wall contractions as a means of predicting a preterm birth (Jacod et al., 2010; Rooijakkers et al., 2014).

The electrohysterogram (EHG) instrumentation, also known as uterine electromyography (EMG), has been seen to be the favoured instrumentation used for the recording of bioelectric signals from the

E-mail address: ennsugbe@yahoo.com.

https://doi.org/10.1016/j.iswa.2022.200123
Received 9 May 2021; Received in revised form 10 July 2022; Accepted 3 September 2022
Available online 7 September 2022

uterine walls (Jacod et al., 2010; Rooijakkers et al., 2014). Also frequently used in conjunction with EHG is the tocodynamometer (Toco) which measures the mechanical uterine contractions, in contrast with EHG which measures the bioelectrical phenomena (HealthManagement.org, 2014). The Toco is comprised of a spring and pressure sensor which is capable of responding to mechanical displacements from uterine contractions (HealthManagement.org, 2014).

The Physionet database, consisting of uterine physiological signals, has helped to accelerate the pace of innovation in this area, with an emphasis on pattern recognition algorithms which can be applied to extract information regarding to foetus condition (Goldberger et al., 2000; Jager, Libenšek & Geršak, 2018, 2018b). Despite this, very little emphasis has been put on the prediction of an associated delivery period upon determining the foetus's condition. As part of an ongoing research work in this area, it was seen that a delivery imminency period estimated in weeks was possible to predict, but the prediction accuracy was seen to degrade when the classifier had to predict a delivery imminency period for foetuses in the early part of their third trimester, likely due to the faint uterine contraction signals associated with the relatively early pregnancy gestations (Nsugbe et al., 2021).

A novel signal decomposition algorithm was designed by the author and previously used in the differentiation of particle sizes in the micron range and for source separation of heterogenous mixtures, where its performance was seen to be superior to the wavelet transform from both an accuracy and real time computational complexity (Nsugbe, 2017; Nsugbe et al., 2018, 2019; Nsugbe et al., 2016; Nsugbe et al., 2016; Nsugbe et al., 2017; Nsugbe et al., 2017). This approach has been recently applied in the area of upper limb prosthesis control for the decoding of phantom motion intent from EMG signals and motor imagery from electroencephalography (EEG) signals from transhumeral amputees, which led to an enhanced recognition accuracy after the application of the decomposition algorithm prior to the classifier training (Nsugbe et al., 2021). Thus, its potential benefits in the decomposition of highly varying physiological signals have been demonstrated.

In this paper, the designed signal decomposition method – referred to herewith as the Linear Series Decomposition Learner (LSDL) – is implemented on the uterine contraction signals to predict a preterm delivery and an associated imminency period for pregnancies in the early part of their third trimester. Specifically, the contributions of this paper are as follows:

- Application of the LSDL alongside a combination of select signal features for preterm and labour imminency prediction using the logistic regression (LR) and support vector machine (SVM) classifiers for both the EHG and Toco instrumentations
- Application of the ReliefF feature ranking algorithm to observe the kinds of features which drive the classification process for both the EHG and Toco

2. Materials and methods

2.1. EHG and Toco

EHG acquires the anatomical action potential resulting from contractions in the form of a bioelectrical signal induced due to biochemical activations during pregnancy (Garfield et al., 2005; Hodgkin & Huxley, 1952; Jyothi et al., 2016; Leitich et al., 1999; Lucovnik et al., 2011; Rihana et al., 2009). Due to the increase in the regularity of contractions that occur in the weeks leading to labour, it can also be said that there is an increase in the dissipation of bioelectric uterine signals from the uterine muscle during this period (Garfield et al., 2005; Hodgkin & Huxley, 1952; Jyothi et al., 2016; Leitich et al., 1999; Lucovnik et al., 2011; Rihana et al., 2009). The effectiveness of the EHG instrumentation is largely pronounced during the third trimester when foetal expulsion is drawing nearer (Cleveland Clinic. n.d.-b, 2022; Human Gestation | Biology for Majors II, n.d.; Medline Plus, n.d.-a; Nierenberg, 2021). EHG is noninvasive and relatively low cost which makes it an appealing option for bioelectric signal acquisition (Garfield et al., 2005; Hodgkin & Huxley, 1952; Jyothi et al., 2016; Leitich et al., 1999; Lucovnik et al., 2011; Rihana et al., 2009).

The Toco instrumentation records the mechanical contraction signals from the uterine muscle contractions with a spring loaded pressure sensor (HealthManagement.org, 2014). Previous work suggests that the Toco is useful in the prediction of preterm births, but as part of this study we would be investigating its effectiveness after the application of the LSDL algorithm (Jager, Libenšek & Geršak, 2018).

2.2. Dataset

The dataset used as part of this paper is from the Physionet database which hosts the EHG and Toco data from a total of 26 patients, 13 of whom delivered term and 13 of whom delivered preterm (Goldberger et al., 2000; Jager, Libenšek et al., 2018, 2018b). All patients provided written and informed consent prior to the recording and the data was collected continuously for 30 min at a rate of 20Hz, and the average gestation period for the preterm patients was 33.7 (± 1.97) weeks, while the average gestation period for the term patients was 38.1 (± 1.04) weeks (Goldberger et al., 2000; Jager, Libenšek et al., 2018, 2018b). Four EHG electrodes were placed around the surface of the uterine muscle, as can be seen in Fig. 1, which in turn produced three signals, while the Toco was placed on the uterine fundus (Jager, Libenšek et al., 2018).

2.3. Signal decomposition

The framework for the LSDL works with a heuristic reasoning framework, where a given time series is sequentially decomposed using a series of tuned linear thresholds as a basis function, alongside a time series peak identification algorithm (Nsugbe, 2017; Nsugbe et al., 2016; Nsugbe et al., 2016; Nsugbe et al., 2017; Nsugbe et al., 2017; Nsugbe et al., 2018, 2019; Nsugbe et al., 2021). For each unique signal decomposition created from altering the amplitude threshold within the time series, a goodness measure exercise is conducted in the form of an optimisation exercise where an optimal decomposition level is

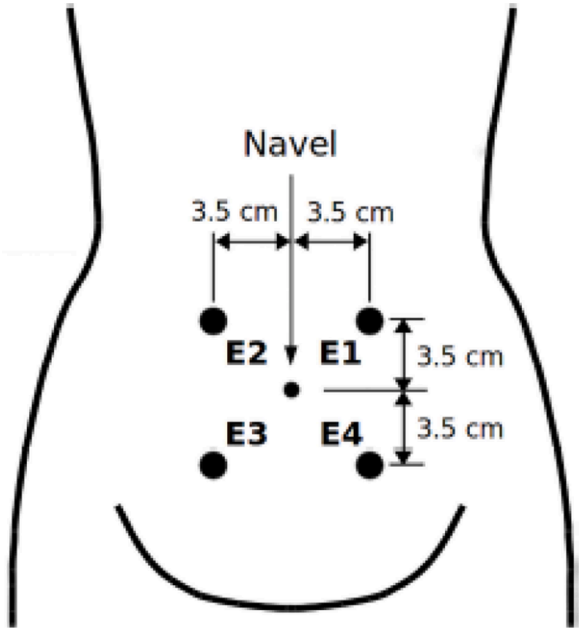

Fig. 1. Electrode placement around the navel with a 7cm spacing (Jager, Libenšek et al., 2018).

determined and selected (Nsugbe, 2017; Nsugbe et al., 2016; Nsugbe et al., 2016; Nsugbe et al., 2017; Nsugbe et al., 2017; Nsugbe et al., 2018, 2019; Nsugbe et al., 2021). The resulting threshold parameters used to decompose the signal to its optimal decomposition level is termed as the optimal threshold and its parameters are stored and termed as X_{opt}, whose parameters are applied towards the decomposition of all further time series signals from the source. A resulting time series which has undergone the LSDL process can be expected to be a reduced dimensional time series which maximises information quality of the phenomena of interest, and thus can be seen as first stage dimensionality reduction prior to feature extraction process (Nsugbe, 2017; Nsugbe et al., 2016; Nsugbe et al., 2016; Nsugbe et al., 2017; Nsugbe et al., 2017; Nsugbe et al., 2018, 2019; Nsugbe et al., 2021).

The LSDL reflects that a linear basis function is used for the decomposition, which is heuristically tuned to yield a series of decomposed sub time series, all of which are subject to an automated learning exercise via a cost function which assesses their classification capabilities.

The following is the list of heuristics required to implement the LSDL and establish the optimal region for a set of distinct time series; $S_1 = x_1, x_2 \ldots . x_N$ and $S_2 = x_1, x_2 \ldots . x_N$, emanating from the same source:

Step 1: Express each time series in its absolute form denoted by $|S_1|$ and $|S_2|$.

Step 2: Apply a unique initialisation threshold to both sets of signals. An arbitrary initialisation adopted from previous work (Nsugbe et al., 2021) has been selected to be 50% of the maximum amplitude of each time series in question, i.e., 50% $*max|x_n|$. This would yield a set of sub time series $\{X_{11_{(upper\ threshold)}}, X_{12_{(lower\ threshold)}}\}$ for each signal from Step 1.

Step 3: For the respective groups of sub time series, a peak identification exercise should be conducted to form $X_{11_{(upper\ threshold)filt}}, X_{12_{filt(lower\ threshold)}}$, where the criteria for a peak is a sample within the time series whose amplitude is either greater than or equal to its nearest neighbours and can be mathematically expressed as $\begin{Bmatrix} x_{peak.n}, x_n \geq x_{n-1}\ and\ x_{n+1} \\ 0,\ Otherwise \end{Bmatrix}$. The role of the peak detection exercise is to eliminate samples within the time series which may be due to interferences during the signal recording process, and therein contribute mainly as a source of uncertainty.

This is followed by a first stage 'fitness' assessment process where the discriminatory capability of each sub time series is calculated. In this work, the mean of peaks (MP) and waveform length (WL) were the features extracted from the relevant sub time series to from a feature vector used to calculate the normalised Euclidean distance metric denoted by J, and acts as the performance index to assess each decomposition region (Phinyomark et al., 2010). Due to the Euclidean distance's sensitivity to scale variations, all values were normalised by the standard deviation of each time series in question, and can be mathematically formulated as follows; S_1 and S_2, assuming Steps 1 and 2 have been applied to the respective time series:

$$ED(p,q) = \sqrt{(p_1 - q_1)^2 + (p_2 - q_2)^2} \tag{1}$$

$$\sigma = \sqrt{\frac{\sum_{w=1}^{N_w} (r_w - \mu)^2}{N_w}} \tag{2}$$

$$J = (p,q) = \frac{ED(p,q)}{\sigma_m} \tag{3}$$

Where ED is the Euclidean distance, p and q are coordinates of the features in the feature vector projected in a Euclidean space from select electrode channels, w is the wth feature within the feature vector, N_w, r_w is a feature within the feature vector, μ is the mean of the feature vector, and σ_m is the mean of the standard deviations of the feature vectors from the two time series (Phinyomark et al., 2010). In order for an efficient and reflective comparison to take place, J should only be calculated for equivalent threshold regions and iterations pairings, for a true reflection; i.e., $\{X_{xy_{filt}\_class S_1}$ and $X_{xy_{filt}\_class S_2}\}$.

Step 4: Subsequent decompositions of $X_{11_{filt(upper\ threshold)}}$, *and* $X_{12_{filt(lower\ threshold)}}$ should follow using the steps defined above, and the threshold tuning parameters in Table 1, until the set stopping criteria have been achieved.

In the case of the subsequent decompositions, only the identified peaks above the set threshold should be considered for all upper thresholds, while only the peaks below tuned lower thresholds should be considered. This rule was set in place as a means of best practice for the LSDL, as was determined from prior studies, and should be adhered to for all further iterations and respective time series decompositions (Nsugbe, 2017; Nsugbe et al., 2016; Nsugbe et al., 2016; Nsugbe et al., 2017; Nsugbe et al., 2017; Nsugbe et al., 2018, 2019; Nsugbe et al., 2021).

The stopping criteria adopted in this work was chosen to be when the number of peaks within a threshold was less than a defined number of samples, which was chosen as six for the sake of statistical robustness. Note that other stopping criteria have been applied in previous studies, and the option of a stopping criteria adds an extra degree of flexibility to the heuristic reasoning based approach which can be modified to suit its immediate application (Nsugbe, 2017; Nsugbe et al., 2016; Nsugbe et al., 2016; Nsugbe et al., 2017; Nsugbe et al., 2017; Nsugbe et al., 2018, 2019; Nsugbe et al., 2021).

Formalisation of the heuristic time series decomposition process can be expressed as a constrained optimisation objective as follows:

$$\text{argmax}(J) \tag{4}$$

$$x_i \in \mathbf{R},$$

Where $\mathbf{R}$ is a set of real numbers, and x_i is a value within the set for values of J evaluated within the n number of sample peaks where the $\text{argmax}(J)$ is selected while taking into consideration values computed from the time series decomposition from both the upper and lower threshold sub time series. The accompanying threshold tuning parameters used to obtain the optimal decomposition region in the time series are identified at this point, and are used to decompose subsequent time series from the same source alongside the peak detection algorithm prior to feature extraction, to maximise class separability during classification exercises. A flowchart of the LSDL can be seen in Fig. 2.

The outcome of the LSDL can be expressed as a superposition of the various decomposition regions alongside the signals and their associated threshold levels. This can ultimately be reconstructed to yield a filtered variant (due to the peak detection algorithm) of the original signal as shown in Eqs. (5)–(7)

$$Upr = \sum_{n=1}^{\infty} T(s)_{l1.upr} + T(s)_{l2.upr} + \ldots\ldots\ldots\ldots T(s)_{ln.upr} \tag{5}$$

$$Lwr = \sum_{n=1}^{\infty} T(s)_{l1.lwr} + T(s)_{l2.lwr} + \ldots\ldots\ldots\ldots T(s)_{ln.lwr} \tag{6}$$

$$S_n = Upr + Lwr \tag{7}$$

2.4. Feature Extraction

The features that were extracted comprise a list which have been previously used in classification exercises of various kinds of physiological signals, alongside an additional list of computationally efficient features which were selected to contribute towards the compensation for not being able to include more nonlinear fractal features (i.e., the Higuchi fractal dimension) due to reduced sample size associated with the LSDL process. The features adopted from previous work include mean absolute value (MAV), WL, slope sign change, root mean square (RMS), sample entropy (SampEN), cepstrum (Ceps), maximum fractal

Table 1
Tuning parameters for the various threshold iterations.

Iteration number	1	2	3	n
Upper threshold region parameter	*Initialisation*/$T_{l\_upper\_1}$ = 50% of max$\lvert S_n\rvert$	$T_{l\_upper\_2} = \frac{\max\lvert S_n\rvert + T_{l\_upper\_1}}{2}$	$T_{l\_upper\_3} = \frac{\max\lvert S_n\rvert + T_{l\_upper\_2}}{2}$	$T_{l\_upper\_n} = \frac{\max\lvert S_n\rvert + T_{l_{upper_{n-1}}}}{2}$
Lower threshold region parameter	*Initialisation*/$T_{l\_lower\_1}$ = 50% of max$\lvert S_n\rvert$	$T_{l\_lower\_2} = \frac{T_{l\_lower\_1}}{2}$	$T_{l\_lower\_3} = \frac{T_{l\_lower\_2}}{2}$	$T_{l\_lower\_n} = \frac{T_{l\_lower\_n-1}}{2}$

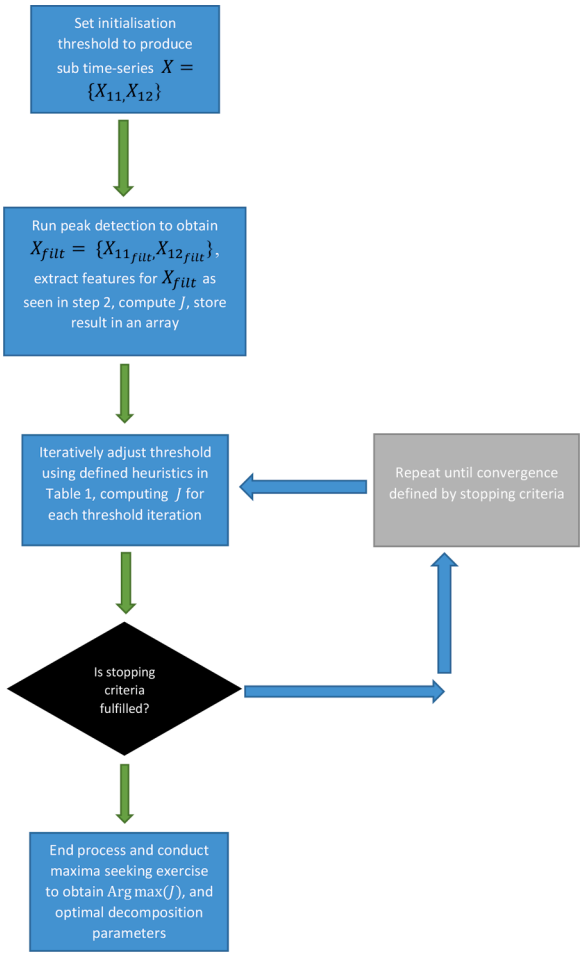

Fig. 2. A flowchart showing the LSDL implementation (Nsugbe et al., 2021).

length (MFL), median frequency (MF), simple squared integral (SSI) and variance (VAR) (Nsugbe et al., 2021). A description and mathematical expression for these features can be seen in Goldberger et al. (2000) and Phinyomark et al. (2010).

The additional list of features includes the following:

- Average Energy (AvEn): provides an indication of the amount of power in the signal and can be mathematically expressed as follows (Too et al., 2019):

$$AvEn = \frac{1}{N}\sum_{n=1}^{N}(x_n)^2 \tag{8}$$

- Modified Mean Absolute Value 1 and 2 (MMAV1 and MMAV2): these sets of features represent a weighted variant of the MAV feature using various weighting rules for various segments of the signal which potentially carry more useful information, thereby amplifying the segment Too et al., 2019). The mathematical expressions for MMAV1 and MMAV2 can be seen in Eqs. (9) and ((10) respectively:

$$\text{MMAV1} = \frac{1}{N}\sum_{n=1}^{N} w_i|x_n| \tag{9}$$

$$w_i = \begin{cases} 1, & if\ 0.25N \le i \le 0.75N \\ 0.5, & otherwise \end{cases}$$

$$\text{MMAV2} = \frac{1}{N}\sum_{n=1}^{N} w_i|x_n| \tag{10}$$

$$w_i = \begin{cases} 1, & if\ 0.25N \le i \le 0.75N \\ \frac{4i}{L}, & if\ i < 0.25N \\ \frac{4(i-L)}{L}, & otherwise \end{cases}$$

Where w_i is the weight window function.

- Log Detector (LD): is a log-based feature which has demonstrated use and applications in the estimation of contraction force associated with muscular contraction, and can be expressed as follows (Too et al., 2019):

$$\text{LD} = \exp\left(\frac{1}{N}\sum_{n=1}^{N}\log(|x_n|)\right) \tag{11}$$

- Skewness: mathematically quantifies the symmetry of a distribution (Nsugbe & Al-Timemy, 2022)

$$\text{Skewness} = \frac{\sum_{n=1}^{N}(n_i-\mu)^3/N}{s^3} \tag{12}$$

Where μ is the mean of the distribution, s is the standard deviation and N represents the number of data points.

- Standard Deviation: gives a quantitative metric of the dispersion associated with a distribution. It can be mathematically expressed as follows (Ng, 2012):

$$\sqrt{\frac{\sum_{n=1}^{N}(x_i-\mu)^2}{N}} \tag{13}$$

- Wilson Amplitude: is a feature used for inferring the action potentials of a set of motor neurons which have fired during the contraction of a muscle, and can be mathematically expressed as follows (Too et al., 2019):

$$\sum_{n=1}^{N} f(x_i) \tag{14}$$

$$w_i = \begin{cases} 1, & if\ |x_i - x_{i+1}| \geq T \\ 0, & otherwise \end{cases}$$

Where T is a user identified threshold.

The threshold value used for all features that required a threshold was 1μv, as used in previous studies (Nsugbe & Al-Timemy, 2022; Nsugbe et al., 2021; Nsugbe et al., 2020), and the parameters for the SampEn were m as 2 and r as 0.2.

2.5. Classifiers

Two candidate classifiers were used in this paper for the classification exercises, namely the logistic regression classifier (LR) and the support vector machine (SVM) (Bishop, 2016; Ng, 2012; Scikit Learn, n.d.). These classifiers were chosen to provide a case study for comparison of classifiers with different architectures and performance with data from the designed decomposition method.

LR: for a binary based decision case formulated as $Y \in \{0,1\}$, function approximation parametrised by θ can be used to infer values of Y, for an input X_i as can be seen in Eq. (15) (Ng, 2012):

$$h_\theta(X) = \frac{1}{1+e^{-\theta^T X}} = \Pr(Y=1|X_i;\theta) \Big/ \Pr(Y=0|X_i;\theta) = 1 - h_\theta(X) \tag{15}$$

Assuming an independently Bernoulli distributed observation, the likelihood function expressed as a log can be formulated as:

$$L(\theta|y;x) = \Pr(Y|X;\theta) \tag{16}$$

$$\prod_i \Pr(y_i|x_i;\theta) \tag{17}$$

$$\prod_i h_\theta(x_i)^{y_i}(1-h_\theta(x_i))^{(1-y_i)} \tag{18}$$

Where x_i is a data sample and y_i is an approximated output.

SVM: this classifier is an iterative classifier which makes it more computationally intense than the LR. It solves an optimisation problem to arrive at an optimal class boundary to separate data clusters (Bishop, 2016; Scikit Learn, n.d.). The discriminant function and optimisation models can be seen in Nsugbe et al. (2021). The cubic kernel expressed as $k(x_i,x_j) = (1+x_i^T x_j)^3$ was used for the term/preterm classification, while the quadratic kernel expressed as $k(x_i,x_j) = (1+x_i^T x_j)^2$ was used for the delivery imminency classifications, with the one vs one multi-class method.

All classifiers were trained using a data split in the order of 70% for training, 15% for validation, and the final 15% as the test set, with the performance evaluated using a K fold cross validation method with the parameter k chosen as 10.

The performance of the classifiers was evaluated using the following four classifier metrics: classification accuracy (CA), sensitivity (Sen), specificity (Spec) and area under the curve (AUC) (Agarwal, 2022).

2.6. Feature ranking

The ReliefF is a filter-based algorithm which is capable of providing a weighted ranking of a group of input features. Since it is a filter-based method (as supposed to wrapper and embedding methods), it is generally computationally efficient as its feature ranking methods are based on indices such as similarities and statistical measures (Kononenko et al., 1997; Urbanowicz et al., 2018). The main shortcoming of this method is its inability to remove or identify feature subsets which may be correlated and thus be providing the same information (Kononenko et al., 1997; Urbanowicz et al., 2018). As the algorithm is being applied primarily for feature ranking purposes and not for feature selection, this limitation does not directly hinder its application in the context of this paper.

The algorithm sorts through a variety of training instances which are labelled, and a score vector is iteratively updated based on the resulting value of the feature difference between the target and neighbouring instances (Kononenko et al., 1997; Urbanowicz et al., 2018). During each iteration, a pair of nearest neighbour instances for the target are identified; one which is within the same class termed as a 'nearest hit' and one which is in a different class termed 'nearest miss' (Kononenko et al., 1997; Urbanowicz et al., 2018). The feature value weights are shortly updated based on whether the value of the feature is different between the target and either one of the nearest hit or nearest miss. In summary, features which possess a different value between the target and the nearest miss are deemed to be informative, thus their weights in the weighting matrix are updated to reflect this (Kononenko et al., 1997; Urbanowicz et al., 2018). While, on the other hand, features which do not reflect the same scenario, have their weights reduced accordingly.

The pseudo code for the ReliefF algorithm can be formulated as follows:

Input: feature vector comprising features and training examples, respective class labels
Set value for m, which reflects the amount of randomly selected training partition used to update the weight vector $\boldsymbol{W}$, and a which is the number of features
Initialise weight vector $W[A]= 0$
for i=1:N
select target instance R_i
seek nearest hit 'H' and nearest miss 'M' instances
for A=1:a
$W[A]= W[A]$ *diff*(A,R_i,H)/N + *diff*(A,R_i,M)/N
end for
end for
return the W vector score containing the quality for each feature

Where the *diff* function is primed towards calculating the difference between values for various instances, and calculate distance between nearest neighbours.

The mathematical formulation for the algorithm can be expressed as follows:

For a set of data points x_r and x_q belonging to the same class:

$$W_j^i = W_j^{i-1} - \frac{\Delta_j(x_r,x_q)}{m}.d_{rq} \tag{19}$$

If x_r and x_q are in different classes then:

$$W_j^i = W_j^{i-1} + \frac{p_{yq}}{1-p_{yr}}.\frac{\Delta_j(x_r,x_q)}{m}.d_{rq} \tag{20}$$

Where W_j^i is the weight of the predictor at the ith iteration, p_{yr} is the prior probability of the class that x_r belongs to, p_{yq} is the prior probability of the class to which x_q belongs, m is the number of updates/iterations, and $\Delta_j(x_r,x_q)$ is the difference in the value of the predictor between the respective observations x_r and x_q. We proceed and define x_{rj} as the jth predictor for the x_r observation and let x_{qj} represent the value jth predictor for the x_q.

The distance function, which is of the Euclidean form, is represented as d_{rq}, defined as $d_{rq} = \frac{\widetilde{d_{rq}}}{\sum_{l=1}^{k}\widetilde{d_{rl}}}$. Where $\widetilde{d_{rq}} = e^{-\left(\frac{rank(r,q)}{sigma}\right)^2}$, and $rank(r,q)$ represents the position of the qth observation in relation to its nearest neighbours of the rth observation sorted with the distance metric. For a discrete prediction $\Delta_j(x_r,x_q) = \begin{cases} 0, x_{rj} = x_{qj} \\ 1, x_{rj} \neq x_{qj} \end{cases}$

2.7. Synthetic minority oversampling technique (SMOTE)

In order to expand the range of data samples used to train the classifier, the SMOTE algorithm was used to generate artificial samples whose characteristics are similar to the already existing dataset using a nearest neighbour criteria (Blagus & Lusa, 2013; Idowu, 2017; Rikunert.

com, 2017).

The following three classification exercises, shown in Table 2, were conducted as part of this paper and the SMOTE algorithm was applied for sample generation and class balancing.

3. Results

Tables 3 and 4 show results from the LSDL for the EHG and Toco, where it can be seen that the greatest perfomance index, and therein the optimal decomposition region, was seen to be in the upper region of the signal for the second iteration. The assumption made is that the optimal decomposition region as determined by the LSDL generalises across other cases involving the signal, i.e., even the optimal decomposition region determined was also utilised in subsequent classification exercises for the prediction of a patient delivery imminency.

Taking into account the value for the performance index *J,* for the raw signal relative to the optimal decomposition region for both signals, it can be seen that the LSDL does provide a substantial enhancement in terms of separability of data samples from different classes, therein boosting the potential classification prowess of the signal.

As mentioned, the classification exercises conducted in this paper include the term/preterm exercise, followed by two delivery week imminency exercises, namely; delivery imminency prediction for signals acquired in gestation weeks 26–29 and delivered preterm, and delivery imminency prediction for signals acquired in gestation weeks 28–31 and delivered term. These two imminency classification exercises were chosen as the results from previous work (Nsugbe et al., 2021) showed that a challenge exists in the prediction of a delivery imminency period for signals acquired in the early part of the third trimester of pregnancy, at <30 weeks of gestation.

Fig. 3 shows the result of the various classification exercises carried out from the EHG (first row) and Toco (second row), for both the SVM and LR classifiers (except for the preterm imminency exercise where only the SVM classifier was used, as this was a 3 class problem, thus rendering the applied architecture of the LR classifier incompatible due to the classes exceeding two). For the term/preterm exercise looking at the EHG and the Toco, the results show that the accuracies for both the SVM and LR are close to 100% across all four classifier metrics, with the EHG appearing to have slight superiority based on the accuracies. For the term imminency exercise, the Toco LR appears to strongly superseed the EHG LR whose accuracies spanned just above the 80% mark, while the Toco LR showed accuracies near to 100%. For the case of the SVM on the preterm imminency for both the EHG and Toco, the classification accuracies appear to be strongly elevated for the EHG, and the Toco undergoes a marginal increase as well. The results for the imminency exercise begin to reinforce that a greater stochasticity exists in electrophysiological signals from the early stage of the third trimester, thus warranting the need for more complex classifiers to separate the various data classes. With the Toco being a mechanical signal and not being prone to attenuation due to anatomical tissue, its resulting signals appear steady enough to be classified using a low complexity classifier such as the LR. This trend is consistent with the preterm imminency results, which were done with the SVM classifier, as this was a 3 class problem. The classification results with the Toco signals outperform the EHG signals in the range of 10–18%, depending on the classifier metric. These results show that the application of the LSDL leads to an enhanced prediction accuracy across all classification case studies considered, and in particular the Toco mechanical signal (and application of LSDL) can be a useful tool and assist the prediction of a labour imminency period for both term and preterm pregnant patients. It is worth mentioning that even though the value for ***J*** in the case of the EHG supercedes that of the Toco, this should not be interpreted as the EHG possessing superior classification performance relative to the Toco as the two types of signals are distinct, due to being bioelectrical and biomechanical signals respectively.

It is worth noting that a concatenation and fusion of the EHG and Toco information was not possible in this paper due to dimensional nonuniformity as a result of the varying sample size of the EHG and Toco data from the Physionet database used in this work, i.e., EHG utilising more channels than the Toco (Goldberger et al., 2000).

Figs. 4–6 show the principal component analysis (PCA) plots with the first two principal components (PCs) for the various classification exercises conducted for both the EHG (left) and the Toco (right). From Fig. 4, a separation can be seen between the respective data clusters, where it can also be noted that there exists more variations in the projections in the EHG plot compared to the Toco, again implying the greater stochasitity of physiological electrophysiological signals relative to mechanical signals. However, it should be noted that the data from the EHG electrodes were from a greater number of electrodes while the Toco data comprised from a single electrode.

For the term imminency exercise from Fig. 5, the Toco PCA plot gives a visual illustration of some of the results encountered in the results plot from Fig. 3, where it can be noted that greater cluster separation occurs for the Toco signals when compared with the EHG signals. The final PCA plot in Fig. 6 shows consistency with the prior plot where the greater cluster separation is seen to occur with the Toco signal relative to the EHG.

Table 5 shows the results of the ReliefF algorithm where the first 10 ranked features are displayed. In the left column EHG Features are displayed, where 7 of the 10 top ranked features (marked with *) are sensitive to the build up of lactic acid in a muscle group, and are termed as 'Fatigue Indices' by Shair et al. (2017). In the case of the Toco features, 6 of the top 10 ranked features are seen to be Fatigue Indices. The results from the feature ranking exercise have shed further insight on the key group of features that contribute the most towards the discriminatory power of the classifiers used for the respective signals. Further work can now include the addition of more Fatigue Indices features in order to further enhance the classification power of the candidate classifiers where applicable.

Table 2
The various classification exercises conducted alongside the number of classes involved.

Classification Exercise	Classes
Term/Preterm	- Term - Preterm
Term imminency for scan conducted in weeks 28–31	- Early Term (weeks 37–38) - Late Term (weeks 39–43)
Preterm imminency for scan conducted in weeks 26–29	- Early Preterm (weeks 29–31) - Mid Preterm (weeks 32–34) - Late Preterm (weeks 35–37)

Table 3
Results of performance index *J* for raw signal and subsequent EHG signal decompositions.

Raw Signal *J*	*J for* $T_{l\_upper\_1}$	*J for* $T_{l\_upper\_2}$
1.055	2.481	3.103
	J for $T_{l\_lower\_1}$	*J for* $T_{l\_lower\_2}$
	2.304	1.031

Table 4
Results of performance index *J* for raw signal and subsequent Toco signal decompositions.

Raw Signal *J*	*J for* $T_{l\_upper\_1}$	*J for* $T_{l\_upper\_2}$
0.199	2.006	2.254
	J for $T_{l\_lower\_1}$	*J for* $T_{l\_lower\_2}$
	2.220	1.457

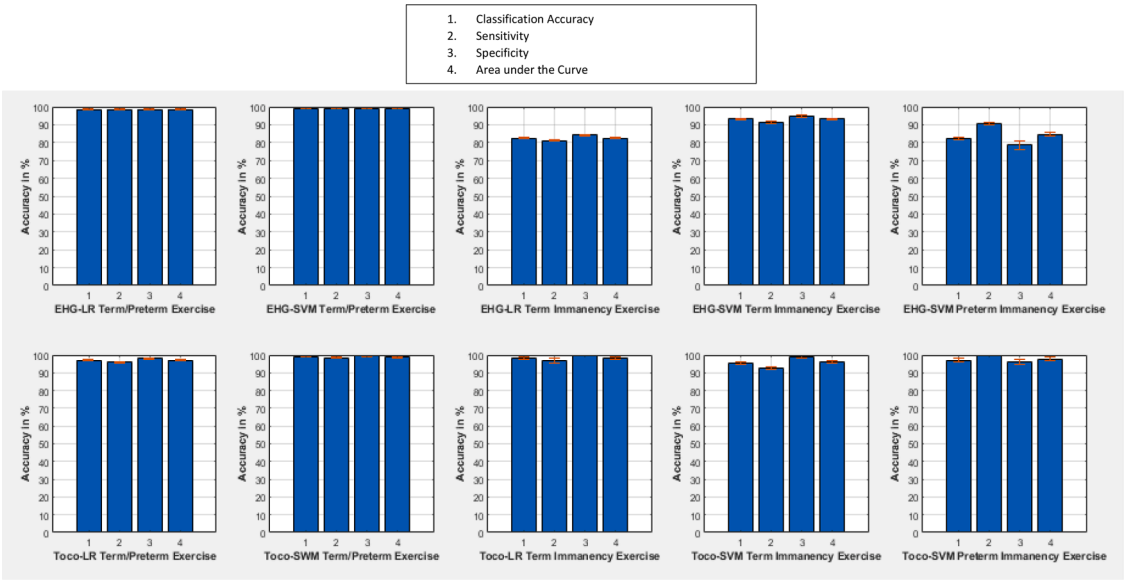

Fig. 3. Results from the various classification exercises.

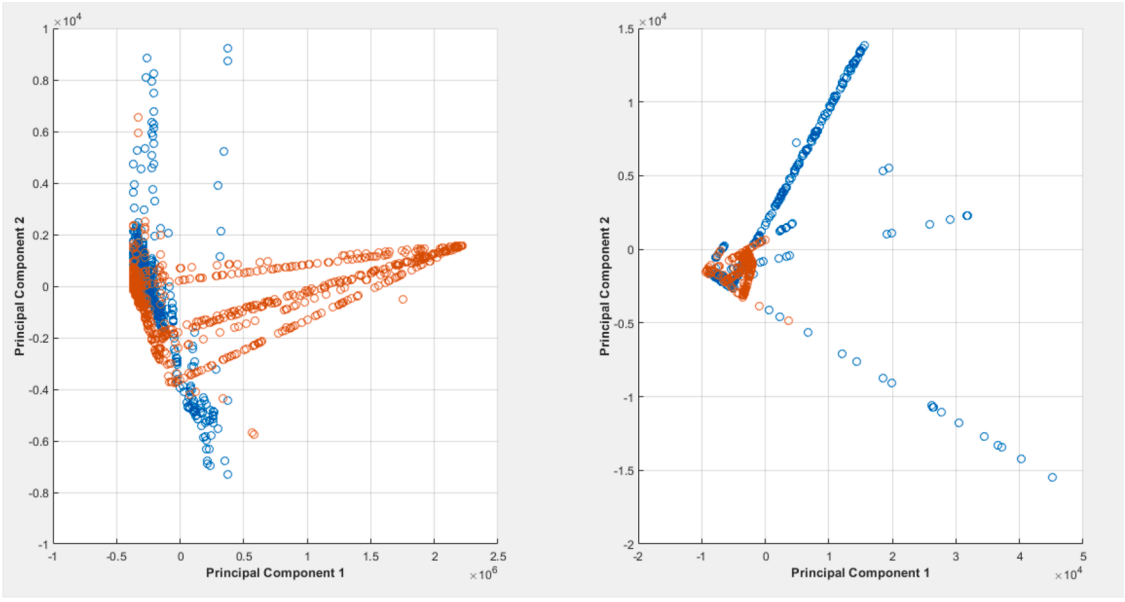

Fig. 4. A PCA plot for the term and preterm classification exercise for the EHG (left) and Toco (right).

4. Conclusion

In this paper, the LSDL has been applied for the preprocessing of the EHG and Toco signals for preterm prediction and select delivery immminency prediction exercises. The LR and SVM classifiers were used, and the benefits of the application of the LSDL has allowed for an enhanced classification across the various metrics considered when compared with a previous study (Nsugbe et al., 2021). In addition to this, the practical benefit of the LSDL includes the need for much less storage space for data, since once the optimal decomposition region within the signal has been identified, all other additional portions of the signal can be discarded. This can be achieved either in software or with the application of analogue clipping circuitry, which can snip the signal in the desired region, and subsequently discard all other portions of the signal as redundant. The main shortcoming of the LSDL method can be seen to be the number of steps and combined sequence required for the determination of the optimal decomposition region, although this can be expected for multiscale signal processing techniques as is also frequently seen with the Wavelet transform.

The classification results for the term/preterm exercise showed a high performance close to 100% for both classifiers and signal types. For the Imminency exercises, the Toco signal appears to provide better accuracy across the different classifiers, thereby implying that mechanical signals appear to provide greater quality signals for pregnant patients in the early phase of their third trimester, which is likely due to the EHG signals being relatively faint and thereby attenuated prior to reaching the surface and the recording instrumentation. The Toco results obtained in this paper have provided further evidence to echo the notion that the instrumentation can indeed be used to provide insights on a potential preterm delivery, the accuracies of which can be enhanced by the use of the presented LSDL signal decomposition method (Jager et al., 2018).

The results from the ReliefF feature ranking exercise showed that a majority of the top ranked features are Fatigue Indices features, thereby

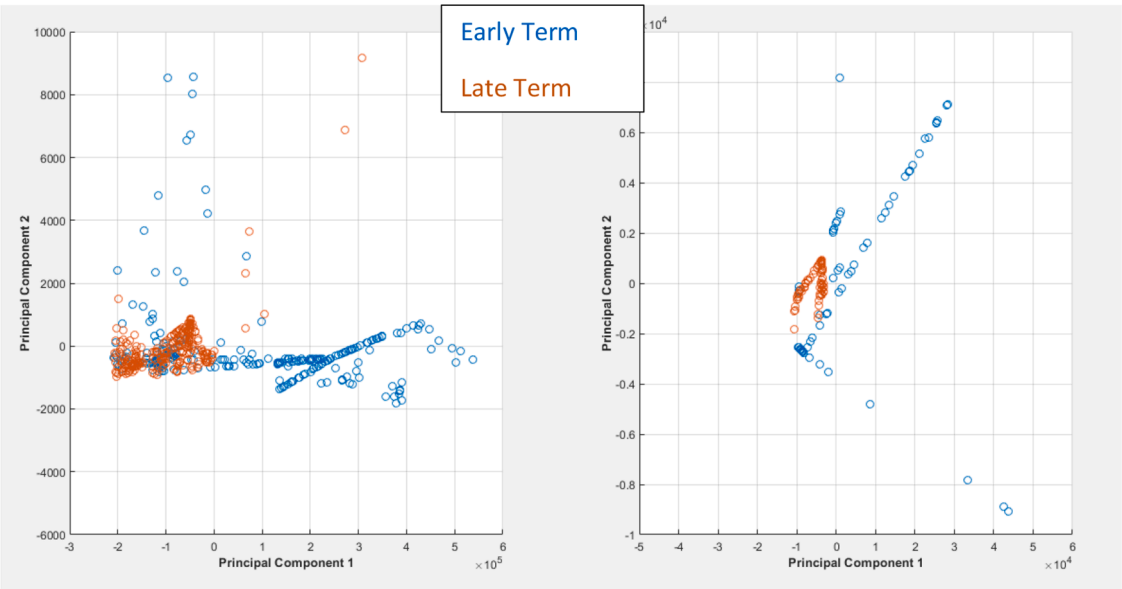

Fig. 5. A PCA plot for the term imminency classification exercise for the EHG (left) and Toco (right).

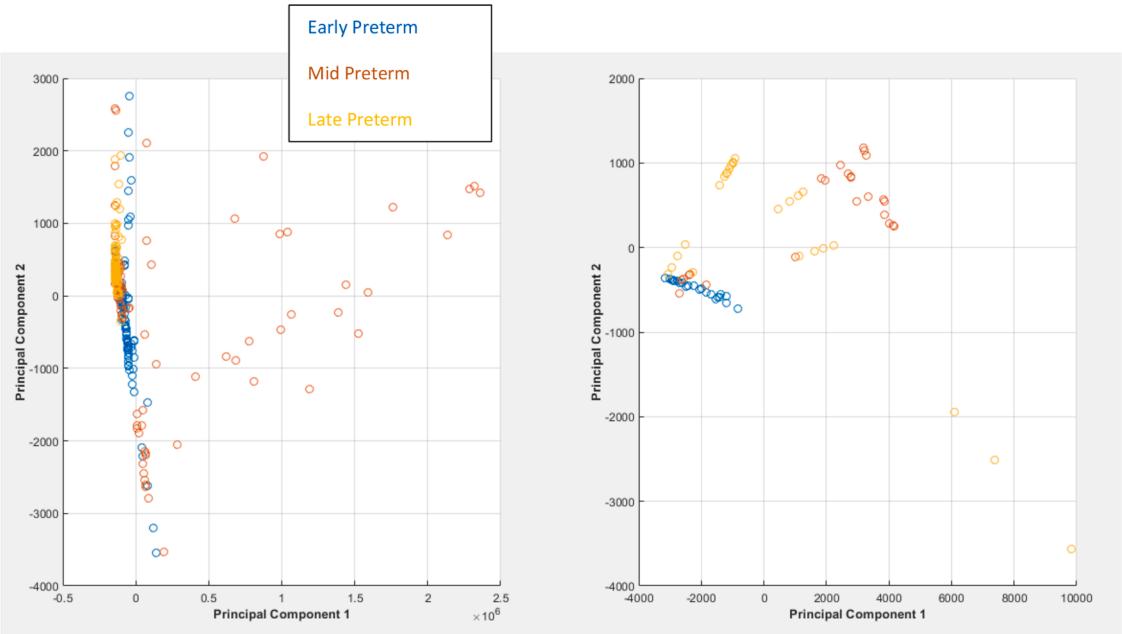

Fig. 6. A PCA plot for the preterm imminency classification exercise for the EHG (left) and Toco (right).

Table 5
Feature ranking results for the highest 10 ranked features with the RelieffF algorithm.

EHG Features	Toco Features
- MMAV2*	- Skewness
- LD*	- Ceps Coeff*
- Med Freq*	- Med Freq*
- MMAV1*	- WL*
- SD	- SSI*
- Ceps Coeff*	- MFL
- MAV*	- SD
- MFL	- Av Energy
- VAR*	- LD*
- RMS*	- RMS*

making apparent the usefulness of these features for classification of these kinds of physiological signal for inferring various medical phenomena.

A key limitation of this work can be seen to be the size of the data utilised for the analysis, which can be said to be relatively small, thus deeming the result to serve as a proof of concept. As part of subsequent work to be carried out, more data would need to be collected from a broader cohort of pregnant women in order to help validate the proposed method and model.

Author statement

Ejay Nsugbe: analysis of data and manuscript draft.

Declaration of Competing Interests

None.

Acknowledgments

This work is in loving memory of Nigel Godwin: even though we interacted only a handful of times, you kindly reminded me of the importance of being thankful for the small things in life each time we spoke.

I would like to thank Dr Michael Provost and Dr Jingwei Too for providing feedback on the manuscript and Brian Kerr from Kerr Editing for proofreading the manuscript.

References

Agarwal, R. (2022). The 5 classification evaluation metrics every data scientist must know. *Medium*.https://towardsdatascience.com/the-5-classification-evaluation-metrics-you-must-know-aa97784ff226, Website-accessed on 12/3/20.

Bishop, C. M. (2016). *Pattern recognition and machine learning (Softcover reprint of the original 1st edition 2006 (corrected at 8th printing 2009))*. New York: Springer.

Blagus, R., & Lusa, L. (2013). SMOTE for high-dimensional class-imbalanced data. *BMC Bioinformatics, 14*(1), 106. https://doi.org/10.1186/1471-2105-14-106

Cleveland Clinic. (n.d.-b). (2022). Fetal development: Month-By-Month Stages of Pregnancy. *Cleveland Clinic*.Retrieved 5 July from https://my.clevelandclinic.org/health/articles/7247-fetal-development-stages-of-growth, Website accessed on 5/7/22.

Figueroa, J. P., Massmann, A., Pimentel, G., & Nathanielsz, P. W. (1987). Characteristics of the electromyogram recorded from the mesometrium of the pregnant ewe from 106 days' gestation to delivery: Similarities with and differences from the Electromyogram obtained from the myometrium. *American Journal of Obstetrics & Gynecology, 157*(4), 991–998. https://doi.org/10.1016/S0002-9378(87)80102-3

Frey, H. A., & Klebanoff, M. A. (2016). The epidemiology, etiology, and costs of preterm birth. *Seminars in Fetal and Neonatal Medicine, 21*(2), 68–73. https://doi.org/10.1016/j.siny.2015.12.011

Garfield, R. E., Blennerhassett, M. G., & Miller, S. M. (1988). Control of myometrial contractility: Role and regulation of gap junctions. *Oxford Reviews of Reproductive Biology, 10*, 436–490.

Garfield, R. E., Maner, W. L., MacKay, L. B., Schlembach, D., & Saade, G. R. (2005). Comparing uterine electromyography activity of antepartum patients versus term labor patients. *American Journal of Obstetrics and Gynecology, 193*(1), 23–29. https://doi.org/10.1016/j.ajog.2005.01.050

Garfield, R. E., Sims, S., & Daniel, E. E. (1977). Gap junctions: their presence and necessity in myometrium during parturition. *Science, 198*(4320), 958–960. https://doi.org/10.1126/science.929182

Goldberger, A. L., Amaral, L. A. N., Glass, L., Hausdorff, J. M., Ivanov, P. Ch., Mark, R. G., … Stanley, H. E. (2000). PhysioBank, PhysioToolkit, and PhysioNet: components of a new research resource for complex physiologic signals. *Circulation, 101*(23). https://doi.org/10.1161/01.CIR.101.23.e215. Website accessed on 13/1/21.

Greenough, A. (2012). Long term respiratory outcomes of very premature birth (<32 weeks). *Seminars in Fetal and Neonatal Medicine, 17*(2), 73–76. https://doi.org/10.1016/j.siny.2012.01.009

HealthManagement.org. (2014). *Radiology Management, ICU Management, Healthcare IT, Cardiology Management, Executive Management*. HealthManagement. https://healthmanagement.org/c/it/news/disposable-tocodynamometer-measures-uterine-contractions, Website accesed on 10/1/21.

Hodgkin, A. L., & Huxley, A. F. (1952). A quantitative description of membrane current and its application to conduction and excitation in nerve. *The Journal of Physiology, 117*(4), 500–544. https://doi.org/10.1113/jphysiol.1952.sp004764

Human Gestation | Biology for Majors II. (n.d.). Retrieved 5 July 2022, from https://courses.lumenlearning.com/wm-biology2/chapter/human-gestation/.

Idowu, I. O. (2017). *Classification techniques using EHG signals for detecting preterm births*. Liverpool: Liverpool John Moores University. Doctoral.

Jacod, B. C., Graatsma, E. M., Van Hagen, E., & Visser, G. H. A. (2010). A validation of electrohysterography for uterine activity monitoring during labour. *The Journal of Maternal-Fetal & Neonatal Medicine, 23*(1), 17–22. https://doi.org/10.3109/14767050903156668

Jager, F., Libenšek, S., & Geršak, K. (2018). *The Term-Preterm EHG DataSet with Tocogram (TPEHGT DS)*. physionet.org. Website accessed on 12/2/21 [Data set].

Jager, F., Libenšek, S., & Geršak, K. (2018). Characterization and automatic classification of preterm and term uterine records. *PLOS ONE, 13*(8), Article e0202125. https://doi.org/10.1371/journal.pone.0202125

Jyothi, R., Soans, R. S., & Bhat, P. V. (2016). Automatic classification of toco-signals: An approach towards comprehensive monitoring of labour progress. *2016 International Conference on Signal Processing and Communications (SPCOM)*, 1–5. https://doi.org/10.1109/SPCOM.2016.7746694.

Kononenko, I., Šimec, E., & Robnik-Šikonja, M. (1997). Overcoming the Myopia of Inductive Learning Algorithms with RELIEFF. *Applied Intelligence, 7*(1), 39–55. https://doi.org/10.1023/A:1008280620621

Leitich, H., Brunbauer, M., Kaider, A., Egarter, C., & Husslein, P. (1999). Cervical length and dilatation of the internal cervical os detected by vaginal ultrasonography as markers for preterm delivery: A systematic review. *American Journal of Obstetrics and Gynecology, 181*(6), 1465–1472. https://doi.org/10.1016/S0002-9378(99)70407-2

Lucovnik, M., Maner, W. L., Chambliss, L. R., Blumrick, R., Balducci, J., Novak-Antolic, Z., & Garfield, R. E. (2011). Noninvasive uterine electromyography for prediction of preterm delivery. *American Journal of Obstetrics and Gynecology, 204*(3). https://doi.org/10.1016/j.ajog.2010.09.024, 228.e1-228.e10.

Marshall, J. M. (1962). Regulation of activity in uterine smooth muscle. *Physiological Reviews. Supplement, 5*, 213–227.

Medline Plus. (n.d.-a). *Fetal development: MedlinePlus medical encyclopedia*. Medline Plus. Retrieved 5 July 2022, from https://medlineplus.gov/ency/article/002398.htm, website accesed on 16/2/20.

Ng, A. (2012). *CS229 Lecture notes*.Akademik.Bahcesehir.Edu.Tr. https://akademik.bahcesehir.edu.tr/~tevfik/courses/cmp5101/cs229-notes1.pdf, website accesed on 13/3/20.

Nierenberg, C. (2021). *Having a baby: Stages of pregnancy by trimester*. Livescience.Com. website accesed on 13/3/20. https://www.livescience.com/44899-stages-of-pregnancy.html

Nikolova, T., Bayev, O., Nikolova, N., & Di Renzo, G. C. (2015). Comparison of a novel test for placental alpha microglobulin-1 with fetal fibronectin and cervical length measurement for the prediction of imminent spontaneous preterm delivery in patients with threatened preterm labor. *Journal of Perinatal Medicine, 43*(4), 395–402. https://doi.org/10.1515/jpm-2014-0300

Nsugbe, E. (2017). *Particle size distribution estimation of a powder agglomeration process using acoustic emissions*.[Thesis] http://dspace.lib.cranfield.ac.uk/handle/1826/14378

Nsugbe, E., & Al-Timemy, A. H. (2022). Shoulder girdle recognition using electrophysiological and low frequency anatomical contraction signals for prosthesis control. *CAAI Transactions on Intelligence Technology, 7*(1), 81–94. https://doi.org/10.1049/cit2.12058. n/a(n/a).

Nsugbe, E., Obajemu, O., Samuel, O. W., & Sanusi, I. (2021). Enhancing care strategies for preterm pregnancies by using a prediction machine to aid clinical care decisions. *Machine Learning with Applications, 6*, Article 100110.

Nsugbe, E., Phillips, C., Fraser, M., & McIntosh, J. (2020). Gesture recognition for transhumeral prosthesis control using EMG and NIR. *IET Cyber-Systems and Robotics, 2*(3), 122–131. https://doi.org/10.1049/iet-csr.2020.0008

Nsugbe, E., Ruiz-Carcel, C., Starr, A., & Jennions, I. (2018). Estimation of fine and oversize particle ratio in a heterogeneous compound with acoustic emissions. *Sensors, 18*(3), 851. https://doi.org/10.3390/s18030851

Nsugbe, E., Starr, A., Foote, P., Ruiz-Carcel, C., & Jennions, I. (2016). Size differentiation of a continuous stream of particles using acoustic emissions. *IOP Conf. Ser.: Mater. Sci. Eng., 161*, Article 012090. https://doi.org/10.1088/1757-899X/161/1/012090

Nsugbe, E., Starr, A., Jennions, I., & Carcel, C. R. (2017). Online particle size distribution estimation of a mixture of similar sized particles with acoustic emissions. *J. Phys.: Conf. Ser., 885*, Article 012009. https://doi.org/10.1088/1742-6596/885/1/012009

Nsugbe, E., Starr, A., Jennions, I. K., & Ruiz-Cárcel, C. (2017). Particle size distribution estimation of a mixture of regular and irregular sized particles using acoustic emissions. *Procedia Manufacturing, 11*, 2252–2259. https://doi.org/10.1016/j.promfg.2017.07.373

Nsugbe, E., Starr, A., Jennions, I., & Ruiz-Carcel, C. (2019). Estimation of online particle size distribution of a particle mixture in free fall with acoustic emission. *Particulate Science and Technology, 37*(8), 953–963. https://doi.org/10.1080/02726351.2018.1473540

Nsugbe, E., Starr, A., & Ruiz-Carcel, C. (2016). Monitoring the particle size distribution of a powder mixing process with acoustic emissions: A review. *Eng. Technol. Ref*, 1–12.

Nsugbe, E., Williams Samuel, O., Asogbon, M. G., & Li, G. (2021). Contrast of multi-resolution analysis approach to transhumeral phantom motion decoding. *CAAI Transactions on Intelligence Technology, 6*(3), 360–375. https://doi.org/10.1049/cit2.12039

Offiah, I., ODonoghue, K., & Kenny, L. (2012). Clinical risk factors for preterm birth. In J. Morrison (Ed.), *Preterm birth—Mother and child*. London: InTech.

Paternoster, D., Riboni, F., Vitulo, A., Plebani, M., Dell'Avanzo, M., Battagliarin, G., Surico, N., & Nicolini, U. (2009). Phosphorylated insulin-like growth factor binding protein-1 in cervical secretions and sonographic cervical length in the prediction of spontaneous preterm delivery. *Ultrasound in Obstetrics and Gynecology, 34*(4), 437–440. https://doi.org/10.1002/uog.6428

Phinyomark, A., Hirunviriya, S., Limsakul, C., & Phukpattaranont, P. (2010). Evaluation of EMG feature extraction for hand movement recognition based on Euclidean distance and standard deviation. *ECTI-CON2010: The 2010 ECTI International Confernce on Electrical Engineering/Electronics, Computer, Telecommunications and Information Technology, n/a*, 856–860.

PMNCH 2012 Progress Report. (2012). *WHO*. World Health Organization. https://pmnch.who.int/resources/publications/m/item/pmnch-2012-progress-report

Rabotti, C., & Mischi, M. (2015). Propagation of electrical activity in uterine muscle during pregnancy: A review. *Acta Physiologica, 213*(2), 406–416. https://doi.org/10.1111/apha.12424

Rihana, S., Terrien, J., Germain, G., & Marque, C. (2009). Mathematical modeling of electrical activity of uterine muscle cells. *Medical & Biological Engineering & Computing, 47*(6), 665–675. https://doi.org/10.1007/s11517-009-0433-4

Rikunert.com. (2017). *SMOTE explained for noobs – Synthetic minority over-sampling TEchnique line by line | Rich Data*. November 15. Rikunert.https://rikunert.com/smote_explained

Rooijakkers, M. J., Rabotti, C., Oei, S. G., Aarts, R. M., & Mischi, M. (2014). Low-complexity intrauterine pressure estimation using the Teager energy operator on electrohysterographic recordings. *Physiological Measurement, 35*(7), 1215–1228. https://doi.org/10.1088/0967-3334/35/7/1215

Scikit Learn. (n.d.). (2022). *1.4. Support Vector Machines*. Scikit-Learn. Retrieved 5 July from https://scikit-learn/stable/modules/svm.html

Shair, E. F., Ahmad, S. A., Marhaban, M. H., Mohd Tamrin, S. B., & Abdullah, A. R. (2017). EMG Processing Based Measures of Fatigue Assessment during Manual Lifting. *BioMed Research International, 2017*, 1–12. https://doi.org/10.1155/2017/3937254

Too, J., Abdullah, A. R., & Saad, N. M. (2019). Classification of Hand Movements based on Discrete Wavelet Transform and Enhanced Feature Extraction. *International Journal of Advanced Computer Science and Applications (IJACSA), 10*(6), 83. https://doi.org/10.14569/IJACSA.2019.0100612. Article 6.

Urbanowicz, R. J., Meeker, M., La Cava, W., Olson, R. S., & Moore, J. H. (2018). Relief-based feature selection: Introduction and review. *Journal of Biomedical Informatics, 85*, 189–203. https://doi.org/10.1016/j.jbi.2018.07.014

van Baaren, G.-J., Vis, J. Y., Grobman, W. A., Bossuyt, P. M., Opmeer, B. C., & Mol, B. W. (2013). Cost-effectiveness analysis of cervical length measurement and fibronectin testing in women with threatened preterm labor. *American Journal of Obstetrics and Gynecology, 209*(5). https://doi.org/10.1016/j.ajog.2013.06.029, 436.e1-436.e8.